Journal of Power Sources 239 (2013) 81–88

Contents lists available at SciVerse ScienceDirect

Journal of Power Sources

journal homepage: www.elsevier.com/locate/jpowsour

Sustainable synthesis of phosphorus- and nitrogen-co-doped porous carbons with tunable surface properties for supercapacitors

Chunlei Wang, Ying Zhou, Li Sun, Peng Wan, Xu Zhang, Jieshan Qiu*

Carbon Research Laboratory, Liaoning Key Lab for Energy Materials and Chemical Engineering, State Key Lab of Fine Chemicals, School of Chemical Engineering, Dalian University of Technology, Dalian 116024, China

HIGHLIGHTS

- P, N co-doped porous carbons have been synthesized by a sustainable approach.
- P, N co-doped porous carbons exhibit tunable surface and textural properties.
- P, N co-doped porous carbons exhibit excellent supercapacitive performance.

GRAPHICAL ABSTRACT

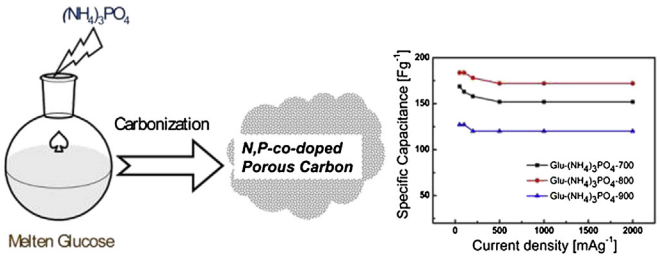

ARTICLE INFO

Article history:
Received 6 January 2013
Received in revised form
2 March 2013
Accepted 23 March 2013
Available online 2 April 2013

Keywords:
Supercapacitor
Sustainable synthesis
Co-doping
Surface properties
Textural properties

ABSTRACT

We report a simple yet efficient method to synthesize phosphorus- and nitrogen-co-doped glucose-derived microporous carbons with a simple inorganic salt (ammonium phosphate) as the single phosphorus and nitrogen source. The obtained products are typical microporous carbons with low surface area and narrow pore size distribution. The doping amount of oxygen, nitrogen, and phosphorus and the population of various functionalities were not only temperature-dependent, but also correlated with each other. The resultant samples exhibit a specific capacitance of 183.8 F g^{-1}, a capacitance retention ratio of over 90%, and an operating voltage up to 1.4 V in an alkaline electrolyte of 6 M KOH. The promising electrochemical performances can be attributed to the synergetic effect of (1) pseudocapacitance that originated from rich and tunable surface group by co-doping of phosphorus and nitrogen; and (2) the electric double layer capacitance that came from the uniform porosities developed by *in situ* activation.

1. Introduction

Carbon materials are currently at the forefront of materials science due to their outstanding electronic, optical, mechanical, catalytic and electrochemical properties, especially in advanced energy conversion and storage fields [1–7]. As one of the most promising energy storage devices, electrochemical capacitor is of great interest due to its large specific energy, high power density, and long durability for applications in hybrid electric vehicles, consumer electronics, or industrial power managements [4]. Despite specific capacitances are lower than that of conducting polymers or metal oxides, porous carbons triumph over their competitors in commercial devices because of their greater cycle stability and higher electrical conductivity [3–6]. Substitution of carbon atoms with heteroatoms (such as nitrogen [8], boron [9], phosphorus [10], and oxygen [11]) in the basal planes and/or at the edges endows them with exciting properties due to the tailored electronic structure and surface properties. Therefore, heteroatom-doped carbons have recently drawn much attention because of their potential applications in metal free heterogeneous catalysis,

* Corresponding author. Tel./fax: +86 411 84986080.
E-mail addresses: jqiu@dlut.edu.cn, clwang@dicp.ac.cn (J. Qiu).

0378-7753/$ – see front matter © 2013 Elsevier B.V. All rights reserved.
http://dx.doi.org/10.1016/j.jpowsour.2013.03.126

solar energy conversion, lithium ion batteries, and fuel cells [12,13]. Incorporation of foreign atom (oxygen [11,14], nitrogen [15], boron [16], sulfur [17], and/or phosphorus [18]) into porous carbon matrix has been proved a practical method to increase the energy density of supercapacitors due to the pseudocapacitance effects originated from Faraday reaction of surface functional groups [15,18,19].

Generally, heteroatom-doped porous carbons are prepared through carbonization of heteroatom-containing synthetic polymer precursors followed by an additional physicochemical activation [20–23] or replication from a hard template through nano-casting processes [24], which are tedious, time-consuming, costly, and harmful to environment. Another approach to prepare heteroatom-incorporated carbons is post treatment of a porous carbon, including surface oxidation, phosphoric acid activation [18,25], ammonia oxidation [26,27], or plasma treatment [28]. Recently, techniques and processes involved in the synthesis of heteroatom enriched porous carbon materials derivate from sustainable precursors have attracted growing interest due to their low cost, energy and atom economy, and low toxicological impact of processes and materials themselves [29]. Oxygen-rich microporous carbons have been prepared through KOH activating of hydrochars derived from biomass (such as cellulose, starch, sawdust, and even fungi) by hydrothermal carbonization (HTC) [30] or one-step carbonization of a seaweed biopolymer [31,32]. Porous nitrogen-doped carbons have been produced by hydrothermal carbonization of chitosan or glucosamine followed by chemical activation [31,33].

The doping amount of heteroatom is dependent on the precursor, the surface chemistry, and the aromatization level of initial carbonaceous supports. Moreover, the development of surface functionalities is dependent on the temperature of heat treatment [34,35]. Understanding the role of heteroatom-containing groups on the electrochemical capacitive properties of carbon electrode is important for the application of the carbon-based supercapacitor. In fact, it is almost impossible to investigate the effect on the capacitive performance of mono heteroatom doping alone except for oxygen, because of the inevitable formation of oxygen-containing functionalities during the development of porosities. In addition, compared with mono heteroatom doping that improves merely one aspect of properties, co-doping (or tri-doping even multi-doping) can enhance overall performance of the materials due to the synergetic effect [36–38]. Therefore, more and more efforts have been focused on understanding the synergetic effects of multi-heteroatom doping in recent years. For nitrogen- and oxygen-co-doping which was extensively investigated, pseudocapacitive Faradic reactions were supposed to take place at the edges of graphene sheets on N-5, N-6 and O-I groups, while N-Q and N-X can help the transportation of electrons [14,18,38]. Recently, D. Hulicova-Jurcakova et al. have demonstrated that phosphorus- and oxygen-co-doping carbons exhibit an extraordinary electrochemical stability [18]. While the widening of the potential window has been accomplished by the blockage of the active oxidation sites with phosphorus groups. In spite of the existence of synergistic effects derived from different heteroatom-containing functionalities was commonly agreed, it is far from fully understood until now. The encountered problem lies in not only the complexity of the carbon surfaces but also the diversified development pathway of the heteroatom-containing surface groups [11,14,18,33,34,38–40]. Post-synthesis approach seems to be one practical way for the preparation of porous carbons with tunable surface properties, but this approach is costly, tedious and time-consuming [14,27,28,40,41].

Herein, we report a simple yet efficient method to synthesize phosphorus- and nitrogen-co-doped microporous carbons with tunable surface properties by using glucose as sustainable precursor and a simple inorganic salt (ammonium phosphate) as the single nitrogen/phosphorus source. Different from post-animated treatment process, the heteroatoms (oxygen, nitrogen, and phosphorus) were doped homogeneously in the whole sample not just at the surface. The introduction of phosphorus into nitrogen- and oxygen-co-doped porous carbons has positive effects on overall capacitive performance and an improvement on the stability through the enhanced textural and surface properties.

2. Experimental

2.1. Materials preparation

In a typical example of synthesis, to a melting glucose (100 g), 80 g $(NH_4)_3PO_4$ was added in small portions within 1 h, and the reaction proceeded for another 4–6 h at 180 °C until foaming ceased. The brown hygroscopic solid was stand still at 180 °C in a muffle furnace for several hours, then 350 °C over night. The resulting solid was carbonized under nitrogen at 700, 800, and 900 °C, respectively. The resulting monolithic foam was crushed into powder, and then washed thoroughly with hot water until neutral. The products were denoted as Glu-$(NH_4)_3PO_4$-700, Glu-$(NH_4)_3PO_4$-800, and Glu-$(NH_4)_3PO_4$-900. For the sake of comparison, their phosphorus-free counterparts have been prepared from glucose with $(NH_4)_3PO_4$ replaced by NH_4Cl, which were named Glu-NH_4Cl-700, Glu-NH_4Cl-800, and Glu-NH_4Cl-900.

2.2. Characterization

X-ray diffraction (XRD, 40 kV, 100 mA) patterns were collected on a Rigaku D/Max2400 diffractometer equipped with a CuKα radiation source. Nitrogen adsorption-desorption measurements were performed at 77 K with a Quantachrome Adsorption Instrument. Prior to the measurements, the samples were degassed at 150 °C for 4 h. The specific surface areas (S_{BET}) were calculated with the Brunauer–Emmett–Teller (BET) equation in a relative pressure range from 0.06 to 0.35. The pore size distributions of the samples were obtained using the non-local density functional theory (NLDFT) approach. The elemental analysis was done by a conventional CHN combustion method (Vario EL-3) based on the burn-off of the sample with a thermoconductive detector (TCD). X-ray photoelectron spectroscopy (XPS, ESCALAB250, Thermo VG Corporation, USA) was used in the surface analyses of the samples. AlKα line (15 kV, 10 mA, 150 W) was used as a radiation source, and the C1s peak position was set at 284.6 eV as an internal standard. The peak separations of the N1s and O1s core level peaks were estimated by least squares with Gaussian–Lorentzian functions after subtraction of background noise. The concentration of each element was calculated from the area of the corresponding peak calibrated with the atomic sensitivity factor using C as the reference. Scanning electron microscopy (SEM) investigations were carried out on a FEI Nova NanoSEM 450 equipped with an Oxford X-MAX energy dispersive X-ray spectroscope (EDS) for elemental analysis.

2.3. Electrochemical measurement

The capacitor electrodes with a diameter of 10 mm were obtained by pressing a mixture of the samples (80 wt%), carbon black (10 wt%) and polytetrafluoroethylene (PTFE) (10 wt%) onto the foam nickel collector. The cyclic voltammetry (CV) and electrochemical impedance spectroscopy (EIS) tests were conducted using an electrochemical working station (CHI660D, Shanghai, China) in a three-electrode cell system, employing a platinum foil as the counter electrode, Hg/HgO as the reference electrode. CVs were recorded between −0.9 and −0.1 V at different scanning rates. The

EIS measurements were carried out in the frequency range of 10 mHz–100 kHz. The Galvanostatic charge-discharge (GC) measurements were conducted on a battery testing system (Land CT 2001, Wuhan, China). The tests were performed in the potential range of −0.9 to −0.1 V at different current densities by a three-electrode system. The specific capacitances (C_g) were calculated from discharge curves according the equation $C_g = I\Delta t/m\Delta V$, where I (A) is the discharge current, Δt (s) is the discharge time, m (g) is the mass of the active carbon material of the single electrode (working electrode), and ΔV (V) is the potential difference during the discharge. All electrochemical experiments were carried out in an aqueous solution of 6 M KOH at room temperature.

3. Results and discussion

The structure and texture properties of samples were first investigated by powder XRD and nitrogen sorption. Phosphorus- and nitrogen-co-doped carbon materials presented a strong amorphous character as confirmed by XRD (Fig. 1(a)). Broad peaks centered at $2\theta = 23$ and 42° were assigned to the graphitic (002) and (101) plane, respectively. The textural properties of samples were analyzed by nitrogen sorption and results were summarized in Table 1. Compared with commercial activated carbons, Glu-$(NH_4)_3PO_4$ series exhibit low S_{BET} of only 197.9, 445.1, 380.2 $m^2\ g^{-1}$, respectively. Glu-NH_4Cl-700 shows a BET surface area of 462.3 $m^2\ g^{-1}$, while S_{BET} decreases rapidly when heat treatment temperature rises to 800 or 900 °C (Table 1). Fig. 1(c) shows nitrogen sorption isotherms of phosphorus- and nitrogen-co-doped carbons carbonized at different temperatures. Glu-$(NH_4)_3PO_4$ series exhibit similarities in the pore structure (type I isotherms) with a high sorption at low relative pressure (P/P_0), which indicates that these carbons are predominantly microporous. While, besides a steep increase at low relative pressure, a slow but continuous increase over a wide range of P/P_0 has been observed for the isotherm of Glu-NH_4Cl-700 (Fig. S1(a)) indicting a board pore size distribution. For obtaining more information on porosity, pore size distribution (PSD) curves are determined by the application of the NLDFT method to the nitrogen sorption isotherms (Fig. 1(d)). Porosities of Glu-$(NH_4)_3PO_4$ series are mainly micropores with a narrow PSD ranging from 0.6 to 1.8 nm. As for Glu-NH_4Cl-700, a much broader size distribution of pores was observed (Fig. S1(b)). The minimum at about 1 nm for both Glu-$(NH_4)_3PO_4$ and Glu-NH_4Cl series can be ascribed to artifacts introduced by modeling assumption [42].

Table 1
EA, surface element distributions obtained from XPS analysis, the BET specific area calculated from nitrogen sorption isotherm, and electrochemical performances of samples.

Sample	EA [%]	XPS [%][a]			S_{BET} [$m^2\ g^{-1}$]	C_g [$F\ g^{-1}$][b]	C_g retention [%][c]
	N	N	O	P			
Glu-$(NH_4)_3PO_4$-700	8.0	5.6	10.2	3.3	197.9	168.8	90.0
Glu-$(NH_4)_3PO_4$-800	4.8	4.0	8.4	2.1	445.1	183.8	93.6
Glu-$(NH_4)_3PO_4$-900	5.4	4.0	9.8	2.9	380.2	127.2	94.4
Glu-NH_4Cl-700	7.8	5.0	3.6	–	462.3	61.0	55.7
Glu-NH_4Cl-800	7.4	4.2	3.9	–	49.7	27.0	48.1
Glu-NH_4Cl-900	6.1	3.9	4.4	–	22.4	20.0	35.0

[a] % of atoms on the surface (mol%).
[b] At the current density of 50 mA g^{-1}.
[c] The capacitance retention ratios were calculated between the current density of 2 A g^{-1} and 50 mA g^{-1}.

Fig. 1(b) shows the FT-IR spectra of samples. Bands at ~3440 cm^{-1} and 1635 cm^{-1} were identified as O–H stretching vibration and C = X (X = C, N, or O) stretching vibration, whilst shoulder peaks at ~3220 cm^{-1} are attributed to N–H stretching vibration. The bands at 1160 cm^{-1} is attributed to C–O stretching and –OH bending modes in ether carboxyl, lactones, P–O–C, and phenolic structures, stretching of P=O groups, and/or stretching of P=OOH; while a band at 1070 cm^{-1} is assigned to the C–N bending mode and/or the symmetry vibration of P–O–P. The decreases of peak intensity at ~1160, 1070, and 755 cm^{-1} (C–H out–of plane bending vibrations of aromatic) when increasing carbonization temperature from 700 to 900 °C indicate the elimination of

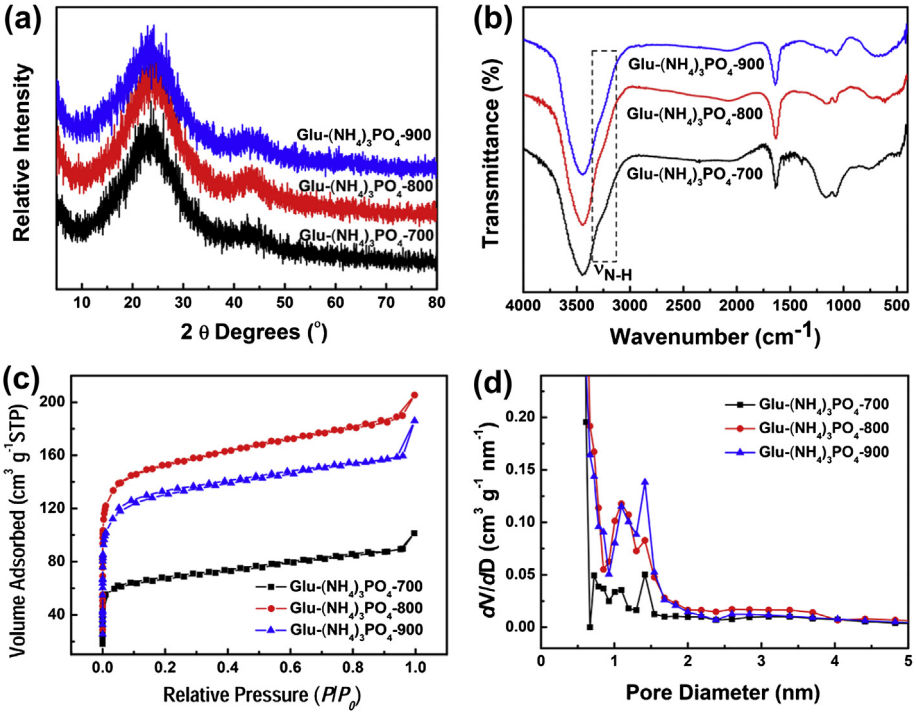

Fig. 1. (a) XRD patterns; (b) FT-IR spectra; (c) nitrogen sorption isotherms; (d) PSDs of phosphorus- and nitrogen-co-doped carbons.

nitrogen-, oxygen-, and/or phosphorus-containing groups as well as the development of aromatization [25,39].

Typical SEM image of phosphorus- and nitrogen-co-doped porous carbon is shown in Fig. 2(b), which confirms the foam nature of the carbon monolith (Fig. 2(a)). Elemental analysis showed phosphorus- and nitrogen-co-doped carbons possess 4.7–8.2 wt% of nitrogen (Table 1). EDX analysis confirms the presence of the oxygen, nitrogen, and phosphorus heteroatom in the carbon matrix (Fig. 2(d)). To investigate the element distribution of these heteroatoms, the EDX mapping was performed. Results (Fig. 2(c)) indicate that oxygen, phosphorus, and nitrogen atoms distribute in the whole sample homogenously.

The incorporation and the surface chemistry of oxygen, nitrogen, and phosphorus elements were further examined by XPS. For phosphorus (Fig. 3(c)), the binding energy around 133.0 eV can be assigned to C–O–PO_3 and/or C–PO_3 groups that commonly occur in phosphoric acid activated carbons [43,44]. Oxygen species (Fig. 3(b)) are represented by peaks at binding energies of around 531.0, 532.0, and 535.0 eV that corresponding to C=O or P=O groups (O-I), C–OH/C–O–C or P–O–C groups (O-II), and chemisorbed oxygen (carboxylic groups COOH) and/or water groups (O-III), respectively. Surface concentrations of oxygen and nitrogen species by fitting the O1s and N1s core level peaks of XPS spectra for all samples were summarized in Table 2. The concentration of oxygen and nitrogen functionalities is temperature dependent. In general, the higher temperature, the lower oxygen (nitrogen) functionalities is expected. As promising precursors for the carbon electrode materials for supercapacitors, saccharides possess high initial oxygen content over 40%, but about only 5% can be preserved in the char after carbonization. Similarly, in this study, surface oxygen contents of Glu-NH_4Cl-700, Glu-NH_4Cl-800, and Glu-NH_4Cl-900 are 3.6, 3.5, and 4.4%, respectively. However, a significant increase of surface oxygen content (over 8.4%) was found in phosphorus- and nitrogen-co-doped carbons due to the introduction of phosphorus (Table 1) [10].

Puziy et al. have proposed the mechanism of high oxygen content for phosphoric acid activated carbons, previously. When using oxygen-enriched biomass (fruit stones) as the precursor, the O/P atomic ratios depend on the temperature of heat treatment [39,43,45,46]. At a low temperature (less than 500 °C), oxygen is bound to the carbonaceous matrix, the decreasing of O/P atomic ratio is attributed to the dehydrating effect of phosphoric acid. However, the proportion of oxygen species that bound to phosphorus increases significantly, when increasing the pyrolysis temperature (600–800 °C), and the value of O/P atomic ratio range from 4 to 3 indicates that most of the oxygen species are P-related. In this work, we believe that most of the oxygen species are P-related because O/P atomic ratios of Glu-$(NH_4)_3PO_4$ series are 3.1, 4.0, and 3.4, respectively. G. Q. Lu et al. have also reported similar results in their recent paper [18].

Oxygen functionalities are most common in porous carbons, which can easily be introduced by various activations. However, not all surface oxygen functionalities are stable; the deterioration of capacitance upon cycling is found to be associated with these unstable surface oxygen groups (O-III) [11,47]. The incorporation of phosphorus into the carbons can inhibit the formation of thus unstable surface groups due to the formation of a protective oxide layer at the surface, which has been verified by temperature programmed desorption (TPD) investigation [10]. As for present work, the O-III groups that formed at a higher carbonization temperature (900 °C) that often causes capacitor instability has been suppressed significantly due to the incorporation of phosphorus (Table 2). Moreover, the contribution of electrochemical active O-I species for phosphorus- and nitrogen-co-doped porous carbon was much higher than that for Glu-NH_4Cl series (Fig. S2(b), Table 2).

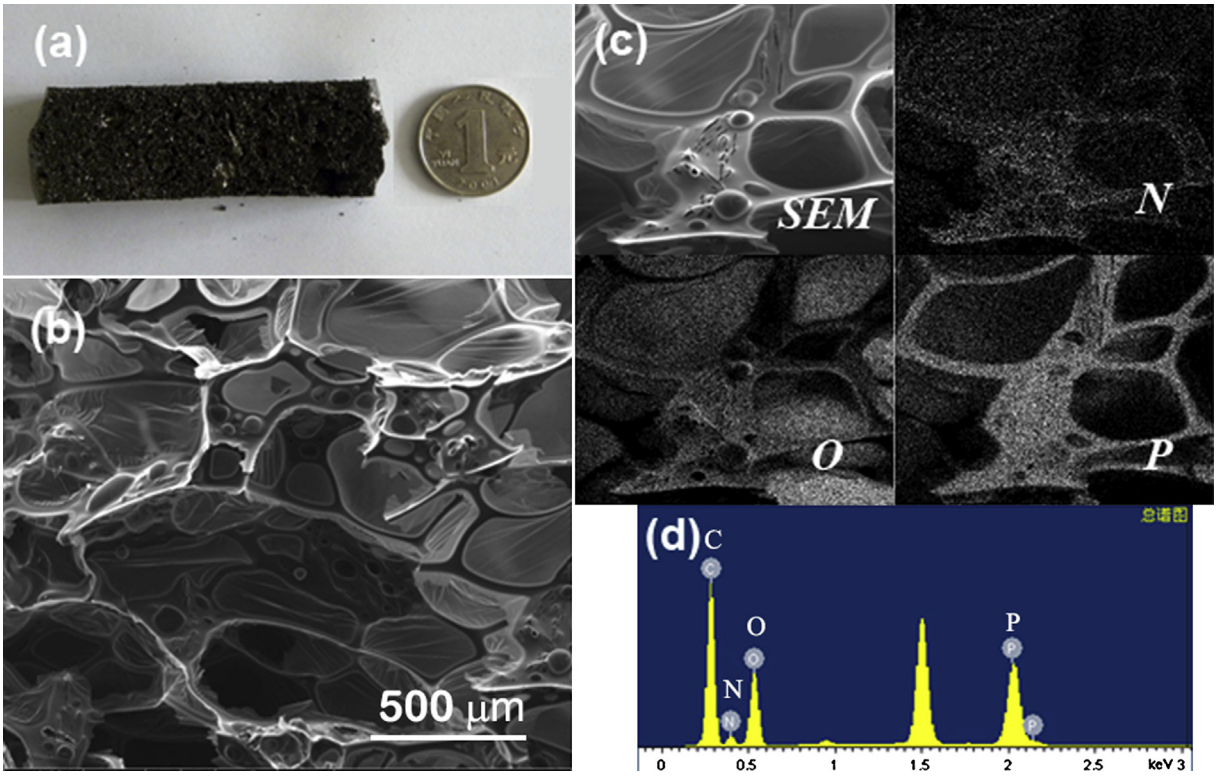

Fig. 2. (a) Optical image and (b) SEM image of a typical piece of carbon monolith; (c) elemental mapping images and (d) EDX spectra of Glu-$(NH_4)_3PO_4$-800.

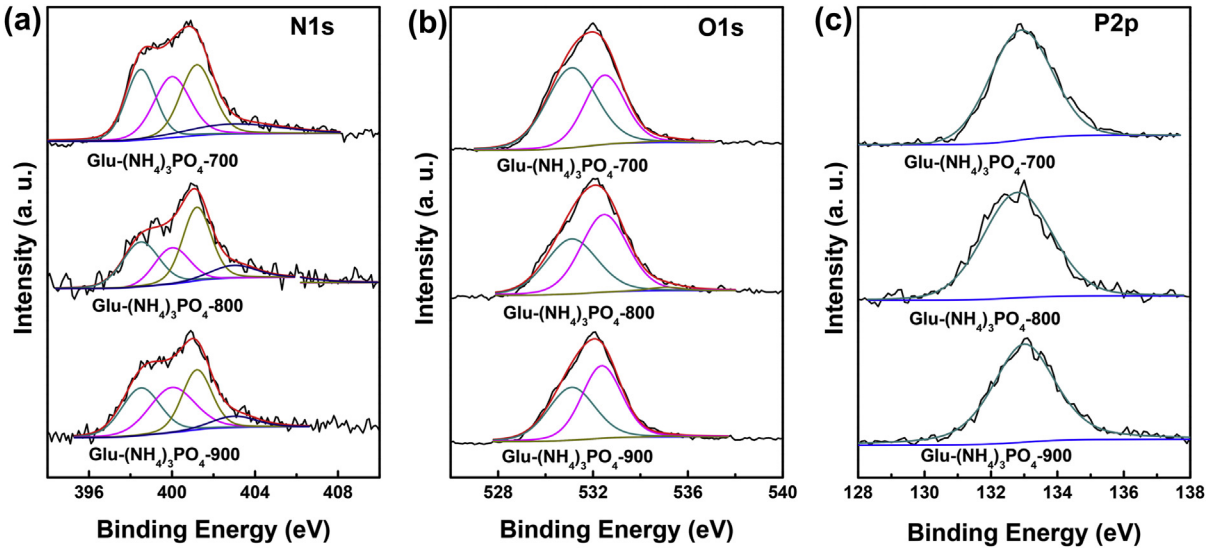

Fig. 3. (a) N1s, (b) O1s, and (c) P2p XPS spectra of Glu-$(NH_4)_3PO_4$ series.

The peaks at 398.5, 400.0, 401.2 and 403.0 eV were identified to pyridinic (N-6), pyrrolic (N-5), quaternary (N-Q) and pyridic-N-oxides (N-X) chemical binding states (Fig. 3(a)), respectively. Negatively charged nitrogen in pyridinic and pyrrolic arrangements can take part in pseudocapacitive Faradic reactions. When distributed in the pores that are accessible to ions, quaternary and pyridic-N-oxides are important for enhancing the capacitance as well. No significant improvement on the surface concentration of N was observed in this work due to the co-doping of P and N (Table 1). Interestingly, relative surface concentrations of pyrrolic N (N-5) in N, P co-doped carbons are much higher than those in their phosphorus-free counterparts (Fig. S2(a), Table 2). Despite the thermal stability of pyrrolic N is still under debate [40,48], similar to Glu-NH_4Cl series in this work, negligible amount of N-5 can be resolved in XPS spectra after high temperature treatment (>750 °C) of nitrogen-containing aerogels that derived from glucose and ovalbumin [35]. Moreover, N-X species that forms at higher temperature (over 750 °C) was suppressed also due to the introduction of phosphorus, which was presumed to the stronger oxygen affinity for phosphorus than for nitrogen (Table 2) [49].

Electrochemical capacitive properties were investigated by means of CV in an aqueous alkaline media (6 M KOH) using three-electrode cells. Fig. 4 (a) and (b) show the CV plots of phosphorus- and nitrogen-co-doped carbons and their phosphorus-free counterparts at a sweep rate of 5 mV s^{-1}. CV curves of mono-nitrogen-doped carbons (Fig. 4(b)) show poor rectangular shapes and small areas that lead to poor capacitive behaviors and low specific conductances. Better rectangular CV plots can be observed for phosphorus- and nitrogen-co-doped carbons (Fig. 4(a)) compared with other biomass (such as sucrose, polysaccharide, fungi, or seaweed biopolymer) derived oxygen-and/or nitrogen-enriched carbon electrodes in alkaline electrolytes [29,30,50]. In addition, the shapes of CV curves retained very well with slight distortions at high voltage scan rates indicating a low equivalent series resistance and a quick diffusion rate of electrolyte ions (Fig. 4(c), and Fig. S3). The C_g calculated from the galvanostatic discharge curves at 50 mA g^{-1} of all samples were displayed in Table 1. The values of 168.8, 183.8, and 127.2 F g^{-1} were obtained for Glu-$(NH_4)_3PO_4$-700, Glu-$(NH_4)_3PO_4$-800, and Glu-$(NH_4)_3PO_4$-900, respectively, which were much higher than those of phosphorus-free counterparts. The specific capacitance of per surface unit (C_{sa}) of Glu-$(NH_4)_3PO_4$-700 is 77.9 μF cm^{-2}, much higher than that of commercial activated carbon (less than 20 μF cm^{-2}) [4], confirming the occurrence of pseudocapacitance associated with rich surface groups. Fig. 4(d) exhibits the relationships between specific capacitance and charge/discharge current density. Specific capacitances of phosphorus- and nitrogen-co-doped carbons decrease slightly with the increase of current density from 50 to 2000 mA g^{-1}, maintaining over 90% of their capacities, much higher than those of mono-nitrogen-doped samples (<56%). Recently, hydrothermal carbonization (HTC) has been proved to be a promising method to synthesize oxygen-rich carbon materials from renewable natural precursors: monosaccharides (glucose, xylose, fructose), and polysaccharides (maltose, sucrose, amylopectin, starch, cellulose), rice, cyclodextrins [29,50], and even fungi [30]. Despite high capacitance of over 250 F g^{-1} can be reached, but the capacitance retention was not satisfied (less than 80%) possibly due to the presence of unstable surface groups [30,32].

The Nyquist plots of the phosphorus- and nitrogen-co-doped carbon-based electrodes are shown in Fig. S4. Glu-$(NH_4)_3PO_4$ series shows straight lines in the low frequency region, which is close to those of ideal capacitors. The semi-cycle at high frequencies is related to the charge transfer resistance and/or the different contact resistances (Fig. S4 insert). The value of equivalence series resistance (ESR) obtained from the point intersecting with the real axis is less than 0.3 Ω, as shown in the inset of the expanded high frequency region of Fig. S4. These demonstrate that phosphorus- and nitrogen-co-doped carbons with a hierarchical pore structure (combination of macropores and uniform micropores, as shown in Fig. 2(b)) can facilitate the mass transfer/diffusion of ions effectively.

It is well known that energy density of supercapacitors is generally lower than that of batteries. The energy density of a supercapacitor is determined by $1/2CU^2$, where C is capacitance and

Table 2
Relative surface concentrations of nitrogen and oxygen species obtained by fitting the N1s and O1s core level XPS spectra.

Sample	N-6	N-5	N-Q	N-X	O-I	O-II	O-III
Glu-$(NH_4)_3PO_4$-700	27.7	29.3	30.9	12.1	58.1	41.1	0.8
Glu-$(NH_4)_3PO_4$-800	30.0	20.9	38.6	10.5	43.2	55.1	1.7
Glu-$(NH_4)_3PO_4$-900	29.9	33.3	28.8	8.0	45.7	54.0	0.3
Glu-NH_4Cl-700	42.9	–	54.1	3.0	8.7	91.3	–
Glu-NH_4Cl-800	39.7	–	48.9	11.4	4.7	95.3	–
Glu-NH_4Cl-900	31.8	–	48.4	19.8	–	94.4	5.6

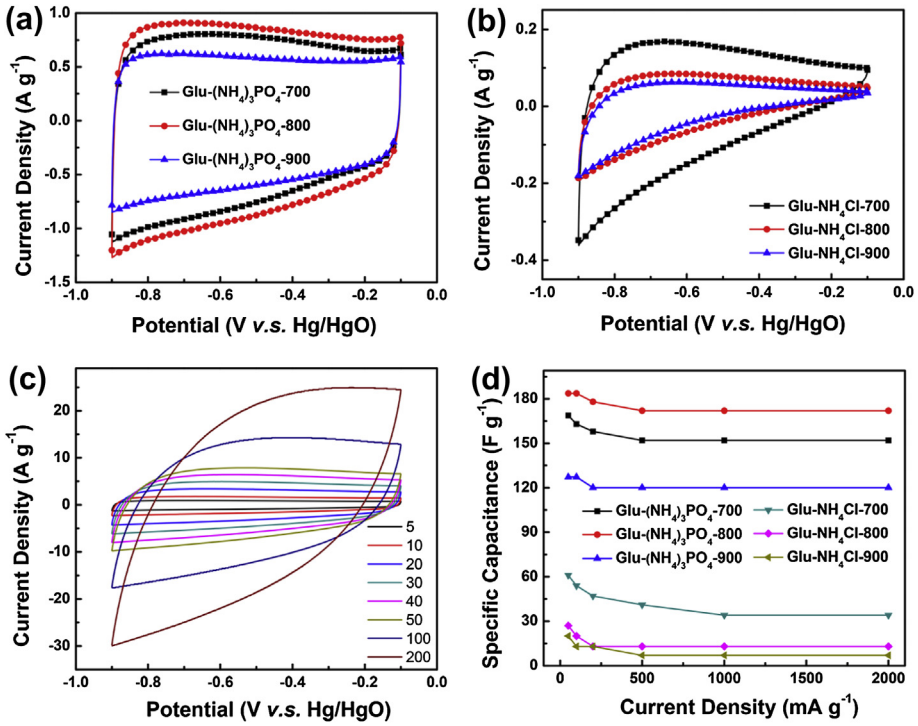

Fig. 4. CV curves of (a) Glu-$(NH_4)_3PO_4$ and (b) Glu-NH_4Cl series at a scan rate of 5 mV s^{-1}; (c) CV curves of Glu-$(NH_4)_3PO_4$-800 at different scan rates from 5 to 200 mV s^{-1}; (d) specific capacitance *vs.* discharge current density plots of the samples.

U is the operational voltage range. Recently, numerous researches are concentrated on the opening of the voltage window, mainly by the use of organic electrolytes. Nevertheless, organic electrolytes are commonly environment-unfriendly, highly viscous, low conductivity and high-cost. Thus, aqueous electrolytes seem to be more competent to supercapacitor application due to their low-cost, safety to operate, and limit environment impact. However, the voltage range of supercapacitors operated in an aqueous electrolyte is limited to 1 V due to H_2O decomposition at 1.23 V. Recently, widening of the cell voltage carbon-based symmetric supercapacitor through oxygen- or phosphorus-doping have been reported [18,38,51]. Fig. 5 shows the cyclic voltammograms of two-electrode cells with Glu-$(NH_4)_3PO_4$-800 and Glu-NH_4Cl-800 based electrodes operated at different potential ranges in 6 M KOH. It is clear that the capacitor built with the Glu-$(NH_4)_3PO_4$-800 can operate at a high potential window up to 1.4 V (Fig. 5(a)), but Glu-NH_4Cl-800 can withstand less than 1 V (Fig. 5(b)).

To investigate the electrochemical stability of phosphorus- and nitrogen-co-doped microporous carbon, the galvanostatic cycling was carried out. Fig. 6 shows the capacitance value vs the number of galvanostatic (1 A g^{-1}) charge/discharge cycles up to 1.3 V for Glu-$(NH_4)_3PO_4$-800 based two-electrode cell in KOH. M. P. Bichat et al. demonstrated that nanostructured carbons with high oxygen content show poor cycle performance in KOH electrolyte [51]. It is reported that the absence of oxygen atoms bonded to carbon in phosphorus-doped carbons is the reason for the long-life cycle performances [18]. Herein, most of oxygen atoms are P-related, therefore Glu-$(NH_4)_3PO_4$-800 with high oxygen content shows well stability, except for a capacitance drop up to ~1500 cycles which can be explain as the presence of the electrochemically active but unstable oxygen groups such as quinone (O-I).

Recently, considerable efforts have been made to understand the combined effect of surface functionalities (pseudocapacitance) and pore structure (EDL capacitance) on the overall capacitive performance [14,38]. Although the exactly mechanism of BET surface area and pore structure on the electrochemical capacitive behaviors is not yet fully understood, they are still the primary factors to the carbon materials for supercapacitor application. Strong dependence of capacitance on the surface nitrogen and oxygen functionalities as well as porosity of carbons has been systematic investigated here. The improved electrochemical capacitive behavior due to the co-doping of nitrogen and phosphorus can be attributed to not only the increasing of the density of surface functionalities that facilitates the formation of pseudocapacitance and the accessibility to ions, but also the uniform microporosities that facilitates the formation of EDLs. It is well known that the pseudocapacitive performances depend on not only the amount of heteroatoms but also the population of the surface functionalities [14,18,38,46]. In this work, a significant increasing in the surface oxygen concentration has been observed due to the introduction of phosphorus. Moreover, the population of nitrogen and oxygen functionalities is strongly dependent on not only the heat treatment temperature but also the introduction of phosphorus. It is worthy noting that the surface concentrations of groups that positive to the capacitance (O-I, and N-5) are increased, but the development of groups relative to the deterioration of capacitors (such as O-III) are suppressed for phosphorus- and nitrogen-co-doping carbons. The improved capacitance retention ratio that relates to the thermal (high temperature treatment) and chemical inhibition (introducing of phosphorus) of unstable oxygen surface species is consistent with previous reports. Correspondingly the widening of the operative voltage for phosphorus- and nitrogen-co-doped microporous carbons can be ascribed to the low unstable oxygen content and the blockage of active oxidation sites by phosphorus groups [18]. Although the present study has identified the impact surface and texture properties of phosphorus- and nitrogen-co-doping on the improvement in capacitive performance, the detail mechanism and the exact roles of phosphorus, nitrogen, and oxygen surface groups still need further investigation.

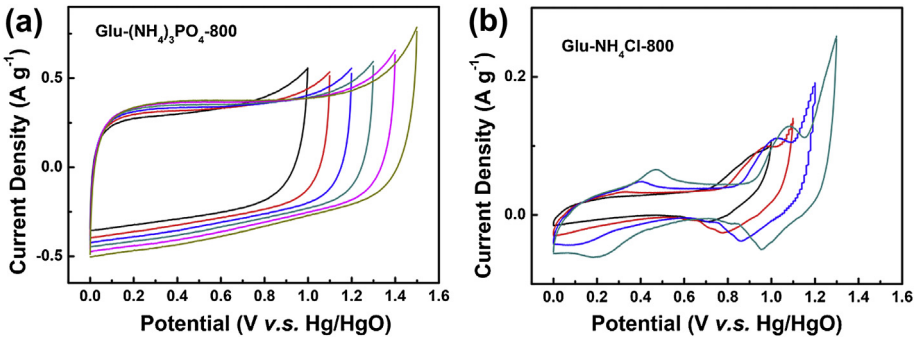

Fig. 5. CVs at 5 mV s^{-1} of symmetric capacitor based on the (a) Glu-$(NH_4)_3PO_4$-800 and (b) Glu-NH_4Cl-800 in 6 M KOH.

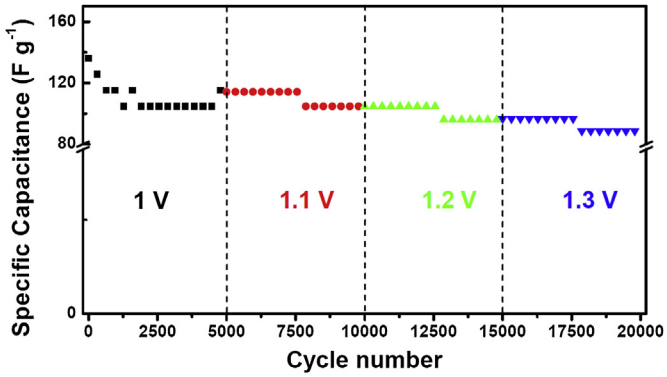

Fig. 6. Cycle performance for P, N co-doped carbon in two-electrode cells (at cell voltages of 1 V–1.3 V).

4. Conclusion

We have demonstrated a feasible, and cost efficient route to the preparation of phosphorus- and nitrogen-co-doped porous carbon materials by using sustainable biomass (glucose) as the precursor. Not only oxygen, nitrogen, and phosphorus surface groups can be introduced into carbon matrix, but also micropores can be developed by *in situ* activation of $(NH_4)_3PO_4$. Interestingly, the amount of heteroatom doped and the development of nitrogen and oxygen functionalities depend on not only the temperature of heat treatment, but also the introduction of the third element P. As a result, the overall amount of surface oxygen increased and the formation of unstable oxygen functionalities at high temperature was significantly inhibited due to the introduction of phosphorus and high temperature thermal treatment. The strong impact of phosphorus on the development of nitrogen and oxygen surface functionalities implies the interrelated development of oxygen, nitrogen, and phosphorus functionalities. The combination of outstanding stability at high current density or high operational voltage and high specific capacitance enables phosphorus- and nitrogen-co-doped carbons to be a promising candidate for high-performance energy storage system. The results could provide new insights into further increasing the capacitance and energy density of supercapacitors and improving their stability. This simple and appealing strategy can easily extended to the synthesis of other co-doped carbons (such as boron and nitrogen) with tunable texture and surface properties. And it is expected that thus obtained multi-element doped carbons with tunable surface and texture properties will find their applications in other advanced energy devices (such as fuel cells, solar cells, and lithium ion batteries) as well as heterogeneous catalysis, besides electrochemical capacitors.

Acknowledgments

The authors are grateful for the support from the National Natural Science Foundation of China (Nos. 21003016, 90610003) and China Postdoctoral Science Foundation (No. 20100481227).

Appendix A. Supplementary data

Supplementary data related to this article can be found at http://dx.doi.org/10.1016/j.jpowsour.2013.03.126.

References

[1] G. Centi, S. Perathoner, ChemSusChem 4 (2011) 913–925.
[2] L.M. Dai, D.W. Chang, J.B. Baek, W. Lu, Small 8 (2012) 1130–1166.
[3] A.G. Pandolfo, A.F. Hollenkamp, J. Power Sources 157 (2006) 11–27.
[4] E. Frackowiak, F. Béguin, Carbon 39 (2001) 937–950.
[5] M. Inagaki, H. Konno, O. Tanaike, J. Power Sources 195 (2010) 7880–7903.
[6] Y. Zhai, Y. Dou, D. Zhao, P.F. Fulvio, R.T. Mayes, S. Dai, Adv. Mater. 23 (2011) 4828–4850.
[7] L.J. Brennan, M.T. Byrne, M. Bari, Y.K. Gun'ko, Adv. Energy Mater. 1 (2011) 472–485.
[8] P. Ayala, R. Arenal, M. Rümmeli, A. Rubio, T. Pichler, Carbon 48 (2010) 575–586.
[9] H. Konno, T. Ito, M. Ushiro, K. Fushimi, K. Azumi, J. Power Sources 195 (2010) 1739–1746.
[10] T. Durkić, A. Perić, M. Laušević, A. Dekanski, O. Nešković, M. Veljković, Z. Lauševi&cacute, Carbon 35 (1997) 1567–1572.
[11] M.J. Bleda-Martínez, J.A. Maciá-Agulló, D. Lozano-Castelló, E. Morallón, D. Cazorla-Amorós, A. Linares-Solano, Carbon 43 (2005) 2677–2684.
[12] Y. Wang, X. Wang, M. Antonietti, Angew. Chem. Int. Ed. 51 (2012) 68–89.
[13] Z.-W. Liu, F. Peng, H.-J. Wang, H. Yu, W.-X. Zheng, J. Yang, Angew. Chem. 123 (2011) 3315–3319.
[14] D. Hulicova-Jurcakova, M. Seredych, G.Q. Lu, T.J. Bandosz, Adv. Funct. Mater. 19 (2009) 438–447.
[15] M. Seredych, D. Hulicova-Jurcakova, G.Q. Lu, T.J. Bandosz, Carbon 46 (2008) 1475–1488.
[16] D.-W. Wang, F. Li, Z.-G. Chen, G.Q. Lu, H.-M. Cheng, Chem. Mater. 20 (2008) 7195–7200.
[17] T. Tsubota, K. Takenaka, N. Murakami, T. Ohno, J. Power Sources 196 (2011) 10455–10460.
[18] D. Hulicova-Jurcakova, A.M. Puziy, O.I. Poddubnaya, F. Suárez-García, J.M.D. Tascón, G.Q. Lu, J. Am. Chem. Soc. 131 (2009) 5026–5027.
[19] X. Zhao, A. Wang, J. Yan, G. Sun, L. Sun, T. Zhang, Chem. Mater. 22 (2010) 5463–5473.
[20] F. Su, C.K. Poh, J.S. Chen, G. Xu, D. Wang, Q. Li, J. Lin, X.W. Lou, Energy Environ. Sci. 4 (2011) 717–724.
[21] K. Leitner, A. Lerf, M. Winter, J.O. Besenhard, S. Villar-Rodil, F. Suárez-García, A. Martínez-Alonso, J.M.D. Tascón, J. Power Sources 153 (2006) 419–423.
[22] S. Villar-Rodil, F. Suárez-García, J.I. Paredes, A. Martínez-Alonso, J.M.D. Tascón, Chem. Mater. 17 (2005) 5893–5908.
[23] K. László, E. Tombácz, K. Josepovits, Carbon 39 (2001) 1217–1228.
[24] C.O. Ania, V. Khomenko, E. Raymundo-Piñero, J.B. Parra, F. Béguin, Adv. Funct. Mater. 17 (2007) 1828–1836.
[25] F. Suárez-García, A. Martínez-Alonso, J.M.D. Tascón, Carbon 42 (2004) 1419–1426.
[26] N.D. Kim, W. Kim, J.B. Joo, S. Oh, P. Kim, Y. Kim, J. Yi, J. Power Sources 180 (2008) 671–675.
[27] K. Jurewicz, K. Babeł, A. Ziółkowski, H. Wachowska, M. Kozłowski, Fuel Proc. Tech. 77–78 (2002) 191–198.

[28] D. Tashima, K. Kurosawatsu, Y.-M. Sung, M. Otsubo, C. Honda, Mater. Chem. Phys. 103 (2007) 158–161.
[29] B. Hu, K. Wang, L. Wu, S.-H. Yu, M. Antonietti, M.-M. Titirici, Adv. Mater. 22 (2010) 813–828.
[30] H. Zhu, X. Wang, F. Yang, X. Yang, Adv. Mater. 23 (2011) 2745–2748.
[31] L. Wei, M. Sevilla, A.B. Fuertes, R. Mokaya, G. Yushin, Adv. Energy Mater. 1 (2011) 356–361.
[32] E. Raymundo-Piñero, F. Leroux, F. Béguin, Adv. Mater. 18 (2006) 1877–1882.
[33] L. Zhao, L.-Z. Fan, M.-Q. Zhou, H. Guan, S. Qiao, M. Antonietti, M.-M. Titirici, Adv. Mater. 22 (2010) 5202–5206.
[34] J.R. Pels, F. Kapteijn, J.A. Moulijn, Q. Zhu, K.M. Thomas, Carbon 33 (1995) 1641–1653.
[35] R.J. White, N. Yoshizawa, M. Antonietti, M.-M. Titirici, Green Chem. 13 (2011) 2428–2434.
[36] P.F. Fulvio, J.S. Lee, R.T. Mayes, X. Wang, S.M. Mahurin, S. Dai, Phys. Chem. Chem. Phys. 13 (2011) 13486–13491.
[37] S. Wang , E. Iyyamperumal , A. Roy, Y. Xue, D. Yu, L. Dai, Angew. Chem. Int. Ed. 50 (2011) 11756–11760.
[38] D. Hulicova-Jurcakova, M. Seredych, G.Q. Lu, N.K.A.C. Kodiweera, P.E. Stallworth, S. Greenbaum, T.J. Bandosz, Carbon 47 (2009) 1576–1584.
[39] A.M. Puziy, O.I. Poddubnaya, A. Martínez-Alonso, A. Castro-Muñiz, F. Suárez-García, J.M.D. Tascón, Carbon 45 (2007) 1941–1950.
[40] P. Nowicki, R. Pietrzak, H. Wachowska, Energy Fuels 24 (2009) 1197–1206.
[41] R. Arrigo, M. Havecker, S. Wrabetz, R. Blume, M. Lerch, J. McGregor, E.P.J. Parrott, J.A. Zeitler, L.F. Gladden, A. Knop-Gericke, R. Schlogl, D.S. Su, J. Am. Chem. Soc. 132 (2010) 9616–9630.
[42] J.P. Olivier, Carbon 36 (1998) 1469–1472.
[43] A.M. Puziy, O.I. Poddubnaya, R.P. Socha, J. Gurgul, M. Wisniewski, Carbon 46 (2008) 2113–2123.
[44] J.M. Rosas, J. Bedia, J. Rodriguez-Mirasol, T. Cordero, Ind. Eng. Chem. Res. 47 (2008) 1288–1296.
[45] A.M. Puziy, O.I. Poddubnaya, A. Martínez-Alonso, F. Suárez-García, J.M.D. Tascón, Carbon 43 (2005) 2857–2868.
[46] J.P. Boudou, P. Parent, F. Suárez-García, S. Villar-Rodil, A. Martínez-Alonso, J.M.D. Tascón, Carbon 44 (2006) 2452–2462.
[47] V. Ruiz, C. Blanco, E. Raymundo-Piñero, V. Khomenko, F. Béguin, R. Santamaría, Electrochim. Acta 52 (2007) 4969–4973.
[48] R. Arrigo, M. Havecker, R. Schlogl, D.S. Su, Chem. Commun. (2008) 4891–4893.
[49] S.-A. Wohlgemuth, F. Vilela, M.-M. Titirici, M. Antonietti, Green Chem. 14 (2012) 741–749.
[50] Z.-L. Xie, R.J. White, J. Weber, A. Taubert, M.M. Titirici, J. Mater. Chem. 21 (2011) 7434–7442.
[51] M.P. Bichat, E. Raymundo-Piñero, F. Béguin, Carbon 48 (2010) 4351–4361.